Time-dependent Analysis of Macro-synthetic FRC Sections with Bar Reinforcement

Author: Raymond Ian GILBERT, UNSW, Australia, i.gilbert@unsw.edu.au
Co-author: Erik Stefan BERNARD, TSE Pty Ltd, Australia, s.bernard@tse.net.au

Topic: Planning and Designing Tunnels and Underground Structures

Keywords: *fibre reinforced concrete, creep, relaxation, design, section analysis*

1. Introduction

Macro-synthetic fibre reinforcement has recently been proposed as reinforcement in several tunnels involving segmental linings internationally. However, concerns have been raised about the long-term performance of macro-synthetic fibres in respect of creep and the associated consequences for crack width development with time under sustained flexural loads. To address these concerns, a method to determine the effects of creep and shrinkage on the time-dependent behaviour of cracked, macro-synthetic fibre reinforced concrete cross-sections containing conventional bar reinforcement subjected to a sustained bending moment and axial force is presented. The analysis is implemented in a spreadsheet and is illustrated by several examples. Although the inclusion of fibres in the concrete has only a minor effect on the flexural strength of the cross-section, the fibres reduce time-dependent in-service deformations and significantly reduce maximum crack widths when used in combination with conventional reinforcing bars.

2. Background

The use of concrete segments is now well established as a means of constructing underground infrastructure. Tunnel segments may be made of plain concrete, but more commonly they include conventional reinforcement or fibre reinforcement. These concrete elements are subject to a wide range of forces and requirements during production, handling, storage, transport, installation, and in service. These requirements will depend on design decisions concerning how and where they are fabricated, how they are transported, and then installed. Most loads imposed on young segments are transitory, and bending moments can usually be kept small relative to bending capacity during production and handling. However, under certain in-service conditions, significant bending moments may possibly be imposed on some segments for a longer period of time. This usually occurs in conjunction with substantial axial (hoop thrust) loads which are almost always sustained in nature. These loading conditions imply that segments will normally be designed for long-term axial hoop loading, and occasionally a combination of sustained axial load and bending moment.

Several alternative methods of design are available for tunnel segments. One can either use engineering first principles, or one of a number of guidelines that purport to represent a consistent set of engineering principles for fibre reinforced concrete (FRC) or reinforced concrete (RC) sections. One such set of principles is embodied in CNR DT 204 [1] which includes fibre reinforcement in combination with conventional reinforcing bars. Other methods include the DBV guideline for steel fibre reinforced concrete (SFRC) [2], or the Model Code 2010 [3]. In each of these guidelines, the tensile capacity of the fibres is modelled as a distributed tensile stress across cracked regions of a section. The fibres can be considered to act on their own or in combination with conventional steel reinforcing bars. The fibres generally provide only a small increase in the ultimate strength of a plain or reinforced concrete cross-section when subjected to significant bending moment in combination with axial compression. However, they increase the post-cracking stiffness of a reinforced concrete section and can significantly reduce deformations and both crack spacing and widths under normal in-service conditions.

All of these design methods for tunnel segments, model an essentially quasi-instantaneous response of a reinforced concrete section to short-term loads and none include provision for the time-dependent effects of creep and shrinkage in the concrete. When a tunnel lining comprises plain concrete, or only fibre reinforcement, and is subject to large axial loads in the absence of significant bending moments, this omission is unlikely to have any noticeable effect on the design outcome. However, if conventional reinforcing bars are included, creep and shrinkage will induce relaxation of stress in the concrete, a gradual transfer of compressive load from the concrete into the bars and a gradual reduction in the cracking moment with time. If fibres are also included in a segment, and the section is expected to be cracked in service, then failure to account for creep and shrinkage can lead to errors in estimation of deformations, crack widths, and stress distributions. To date, steel fibres have been used in the majority of FRC segmental tunnel linings, but in more recent times, macro-synthetic fibres have been considered as a viable substitute. Although providing economic advantages and improved durability, concerns over long-term crack widths have often been raised as an obstacle to the use of macro-synthetic fibres in tunnel segments. The time-dependent behaviour of macro-synthetic fibre reinforcement under a sustained bending moment on a cracked section has hitherto received little research attention.

The importance of creep and shrinkage to the long-term behaviour of reinforced and prestressed concrete sections is well known and models for predicting these time-dependent deformations and stress redistribution are well established [4]. Failure to account for the effects of creep and shrinkage can lead to serious under-estimation of the extent and severity of cracking, as well as long-term deformations. Since the loads imposed on tunnel segments are similar in nature to the sustained axial and flexural loads normally applied to prestressed girders, existing methods for the creep and shrinkage analysis of prestressed concrete can be readily extended to FRC tunnel segments. This paper describes a method of analysis to determine the effects of creep and shrinkage on the time-dependent behaviour of cracked, macro-synthetic fibre reinforced concrete cross-sections containing conventional bar reinforcement and subjected to a sustained bending moment and axial force. The method of analysis and the material modelling are described, and typical numerical results are presented. The fibre-reinforced concrete considered in the analysis consists of macro-synthetic fibres mixed into normal or high strength concrete, but the analytical model can also be used for concrete with steel and other types of fibres. The presence of the fibres enhances the post-cracking tensile strength of the concrete and improves the ductility of the material.

The cross-section is modelled by dividing the depth of the cross-section into 50 layers of equal thickness. Conventional bar reinforcement can be included at any point on the cross-section. Stresses and deformations caused by the applied loads, and by creep and shrinkage of the concrete and relaxation of the fibres, are determined at 11 time instants, (τ_0 to τ_{10}), with τ_0 being the time when the bending moment and axial force are first applied to the cross-section and τ_{10} is the final time instant when the final stresses and deformations are required. Internal actions are assumed to be constant in time. The extent of cracking is determined at first loading (i.e. at τ_0) and the time-dependent deformations and stress redistribution on the cracked section are calculated in each subsequent time step using the principle of superposition and a step-by-step method of analysis [4].

3. Assumed constitutive relationships

3.1 Fibre-Reinforced Concrete

At any time t, the total concrete strain $\varepsilon_c(t)$ at a point on the cross-section is assumed to be the sum of the instantaneous strain $\varepsilon_{ce}(t)$, the creep strain $\varepsilon_{cc}(t)$, and the shrinkage strain $\varepsilon_{cs}(t)$. Although not strictly correct, it is usual to assume that all three components are independent and may be calculated separately and combined to obtain the total strain. In the present analysis, the value of each strain component is determined at the centroid of each concrete layer at each time instant (τ_0 to τ_{10}), together with the concrete stress. For convenience in subsequent notation, the argument (t) will be omitted when describing strain components. Creep and shrinkage strains are assumed to begin to develop in each layer immediately after first loading at τ_0 and continue until time τ_{10}.

3.1.1 Instantaneous strain

In compression: Under in-service conditions, the compressive stress in the concrete rarely exceeds about 0.5 times the compressive strength and the shape of the stress strain curve is essentially linear. In this low-stress range, the secant modulus E_{cc} does not vary significantly with stress and is only slightly smaller than the initial tangent modulus. The instantaneous stress-strain relationship is therefore assumed to be linear-elastic (i.e. $\varepsilon_{ce} = \sigma/E_{cc}$). Although the elastic modulus increases with time, as the concrete gains strength, and also depends on the rate of application of the stress, for most practical purposes, these variations are usually ignored in practice. In this study, we assume that E_{cc} is constant with time and equal to its value at the time of first loading, τ_0. The value of the elastic modulus in compression E_{cc} is largely independent of the fibre content and may be determined by tests or by well-established formulas for plain concrete [5, 6, 7].

In tension: The tensile strength of concrete is variable and the behaviour after cracking is highly dependent on the type, quantity and orientation of fibres crossing the crack. Experimental results for the instantaneous loading-unloading-reloading behaviour of macro-synthetic FRC is shown in Fig. 1a. This indicates a typically complex behaviour, with a unload-reload modulus that depends on the loading history and total sustained strain. Such behaviour can be idealised using the model shown in Fig. 1b, but even this simplification requires complex tracking of the post-crack strain history for the FRC and is thus too complex to include in a spreadsheet.

As an alternative, the far simpler instantaneous response in tension shown in Fig. 2 is assumed in the current analysis. Up until first cracking, the instantaneous response is assumed to be linear elastic. Cracking occurs when the stress reaches the tensile strength of concrete f_t' at a strain $\varepsilon_{t.1}$. In the absence of more accurate information, the elastic modulus in tension before cracking E_{ct} is here assumed to be equal to E_{cc}. At first cracking, the stress drops sharply and the fibres begin to carry tension across the crack. This conservative model represents the *average* stress-instantaneous strain relationship observed in tests after cracking with an envelope that is similar to the peak curve shown in Fig. 1a. The residual tension is carried by the fibres as strain increases after cracking $f_{t.r}'$ and depends on the quantity and properties of the fibres used in the mix. The magnitude of the residual strength is best determined from tests.

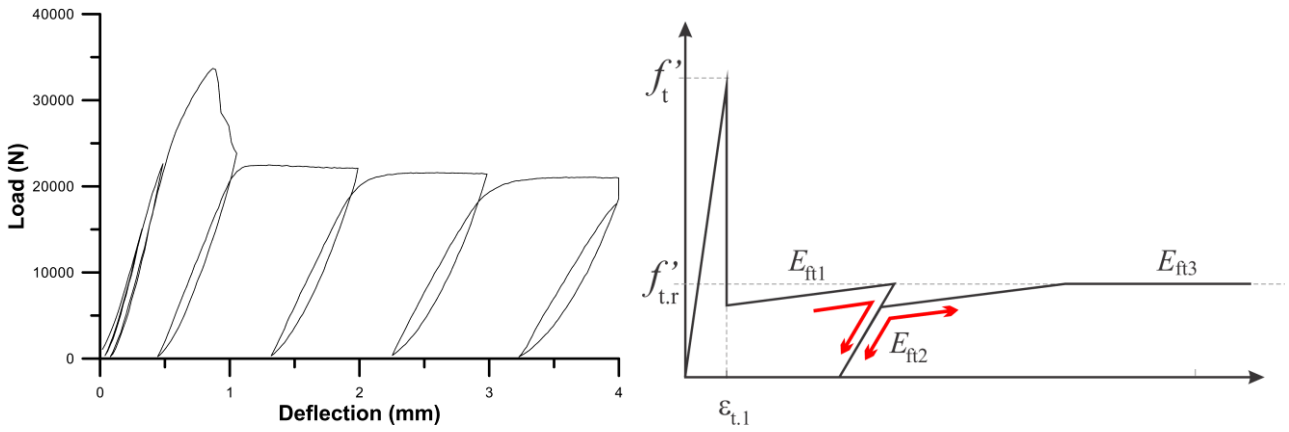

Fig. 1 a) Test data for macro-synthetic FRC under cyclic loading, and b) idealised stress-strain relation for macro-synthetic fibre-reinforced concrete in tension.

In the analysis presented here, the saw tooth shaped stress-strain relationship shown in Fig. 2 is adopted to represent the post-cracking behaviour of the fibre reinforced concrete. The residual tension $f_{t.r}'$ is taken as $(0.4 f_t' \rho_f / 6)$ where ρ_f is the fibre content in kg/m^3, i.e. $f_{t.r}' = 0.2 f_t'$ and $0.4 f_t'$ when ρ_f = 3 kg/m^3 and 6 kg/m^3, respectively. After cracking, the effective modulus of the fibre concrete progressively reduces as strain increases, with six values (E_{ft1} to E_{ft6}) used in the spreadsheet analysis to represent the fibre response after cracking, as shown.

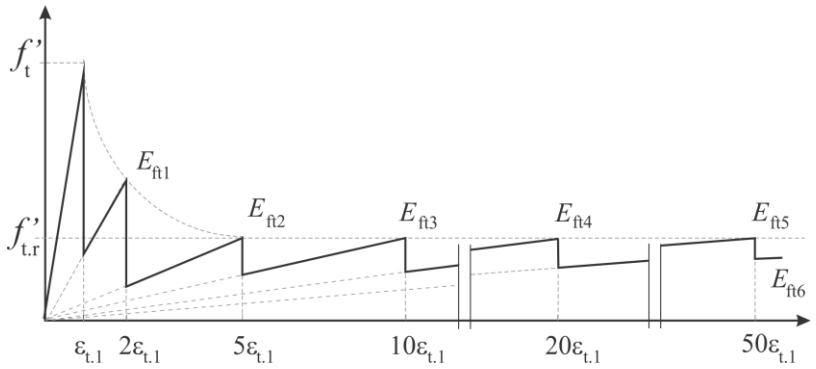

Fig. 2 Assumed stress-instantaneous strain curve for fibre-reinforced concrete in tension.

3.1.2 Creep of Fibre-Reinforced Concrete

In uncracked layers: For concrete subjected to a constant sustained stress, creep strain increases at a decreasing rate. In the period immediately after first loading, creep develops rapidly, but the rate of increase slows appreciably with time. After several years under load, the rate of change of creep with time is small. Discussions of the mechanisms causing creep and the factors affecting its magnitude and rate of development are available elsewhere [4, 8, 9, 10]. In addition to the environment and the characteristics of the concrete mix, creep depends on the stress history, in particular the magnitude and duration of the stress, and the age of the concrete when the stress is first applied τ_0. Concrete loaded at an early age creeps more than concrete loaded at a later age. Compressive stresses rarely exceed $0.5 f_c^{'}$ in concrete structures at service loads, and at these stress levels, creep may be assumed to be proportional to stress.

The capacity of concrete to creep is usually measured in terms of the creep coefficient, φ_{cc}. In a concrete specimen subjected to a constant sustained compressive stress, σ_c, first applied at age τ, the creep coefficient at time t is the ratio of creep strain to instantaneous strain and is given by:

$$\varphi_{cc}(t,\tau) = \varphi_{cc} = \varepsilon_{cc} / \varepsilon_{ce} \quad (1)$$

Therefore, the creep strain at time t caused by a constant sustained stress σ_c first applied at age τ is

$$\varepsilon_{cc} = \varphi_{cc}\, \varepsilon_{ce} = \varphi_{cc}\, \sigma_c / E_{cc} \quad (2)$$

where E_{cc} is the elastic modulus at time τ. For concrete subjected to a constant sustained stress, knowledge of the creep coefficient allows the rapid determination of the creep strain at any time.

Since, in the present analysis, we have also assumed that both the creep and the instantaneous strain components are proportional to stress at in-service stress levels in the uncracked concrete, the creep coefficient φ_{cc} is a pure time function, independent of the applied stress and increases with time at a decreasing rate. It is also assumed in the present analysis that the creep of uncracked concrete is the same in tension and compression. Although there is some evidence that the creep coefficient increases indefinitely for concrete in compression, its final value φ_{cc}^{*} is often taken as the 30 year value and its magnitude usually falls within the range 1.5 to 4.0. A number of well-known methods for predicting the creep coefficient of concrete without fibres are available [5, 6, 7] and these are suitable for the uncracked fibre-reinforced concrete.

In the cracked concrete layers: The previous discussion has concerned the creep of concrete in the uncracked concrete in both compression and tension. In a cracked concrete layer, *smeared* rather than *discrete* cracking is assumed and average deformations are determined over a gauge length containing several cracks. In reality, after cracking when strain exceeds $\varepsilon_{t.1}$ (see Fig. 2), the residual tensile stress at a crack is carried by macro-synthetic fibres and, between the cracks, the residual stress is carried by the uncracked concrete. The average creep strain that develops in the cracked layer can therefore be modelled using an average creep coefficient $\varphi_{cf.av}$ (averaged between the creep coefficients for the macro-synthetic fibres and the uncracked concrete in tension). The magnitude and rate of

development of this average creep coefficient is best determined by testing. Preliminary testing has suggested that the magnitude of $\varphi_{cf.av}$ at any time is significantly greater than φ_{cc} for the uncracked concrete. The creep that develops in a cracked layer may also be obtained by substituting $\varphi_{cf.av}$ for φ_{cc} in Eq. 2.

3.1.3 Shrinkage Strain of Fibre-Reinforced Concrete:

Shrinkage of concrete is the time-dependent strain in an unloaded and unrestrained specimen at constant temperature. Shrinkage of the hardened concrete is often divided into two components, *chemical* shrinkage and *drying* shrinkage. *Drying shrinkage* is the reduction in volume caused principally by the loss of water during the drying process. *Chemical shrinkage* (or *autogenous shrinkage*) results from various chemical reactions within the cement paste and includes hydration shrinkage that is related to the degree of hydration of the binder in a sealed specimen with no moisture exchange. Chemical shrinkage (often called) occurs rapidly in the days and weeks after casting and is less dependent on the environment and the size of the specimen than drying shrinkage. In the absence of test data for fibre-reinforced concrete, methods for predicting the unrestrained linear shrinkage of concrete without fibres (ε_{cs}) are available and these are also suitable for fibre-reinforced concrete [5, 6, 7].

3.2 Steel Reinforcing Bars

Steel is modelled as elastic perfectly plastic. Prior to yielding, the steel reinforcing bars are assumed to be linear elastic in both compression and tension, i.e. $\sigma_s = E_s\varepsilon_s$, where E_s is the elastic modulus of the steel. In the absence of test data, E_s is taken to be 200×10^3 MPa, irrespective of the type and Ductility Class of the steel. Alternatively, E_s may be determined from standard tests. The elastic modulus in compression is taken to be identical to that in tension. It is the in-service behaviour of the cross-section that is being modelled here and steel stresses at service loads are generally less than the yield stress.

4 Cross-sectional analysis

4.1 Overview

The governing equilibrium equations describing the behaviour of the cross-section are expressed in terms of the two unknowns that define the strain diagram, i.e. the strain at the reference axis ε_r and the slope of the strain diagram κ (which is the curvature of the cross-section). The reference axis is taken as the centroidal axis of the uncracked cross-section.

Consider the typical cross-section shown in Fig. 3a. The section is symmetric about the *y*-axis and the orthogonal *z*-axis (the centroidal axis of the uncracked cross-section) is taken as the reference axis. Based on the right-hand rule, the positive *x*-axis is directed out of the page. If the cross-section is subjected to an axial force applied at the origin of the *z* and *y* axes (tensile (+ve) in the direction of the *x* axis) and a bending moment applied about the *z*-axis, the strain diagram is shown in Fig. 3b. The strain at any height *y* above the reference axis is given by:

$$\varepsilon = \varepsilon_r - y\kappa \tag{3}$$

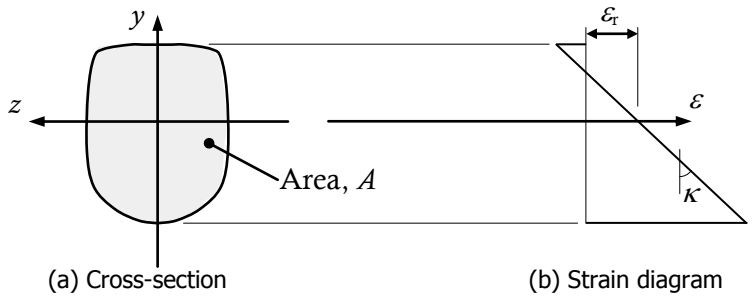

Fig. 3 Generic cross-section

The two unknowns, ε_r and κ, are determined by enforcing horizontal and rotational equilibrium at the cross-section:

$$N_{\mathrm{i}} = N_{\mathrm{e}} \quad \text{and} \quad M_{\mathrm{i}} = M_{\mathrm{e}} \tag{4a, b}$$

where N_e and M_e are the external axial force and moment, respectively, at the section and N_i and M_i are the internal axial force and moment, respectively, given by

$$N_{\mathrm{i}} = \int_A \sigma \,\mathrm{d}A \quad \text{and} \quad M_{\mathrm{i}} = \int_A y\sigma \,\mathrm{d}A \tag{5a, b}$$

When the strain distribution is determined, the stresses in the concrete and steel may be obtained from the appropriate constitutive relationships. This procedure forms the basis of both the short- and long-term analyses presented in the following.

4.2 The layered cross-section:

For the short-term and time-dependent analyses of a rectangular cross-section of width b and overall depth D, the cross-section is partitioned into 50 layers of equal thickness through the depth of the section, as shown in Fig. 4. The thickness of each layer t_c is therefore equal to $D/50$. Although any number of levels of reinforcement can be included, we will consider just two levels as shown in Fig. 4. The area of reinforcement at each level is A_{s1} and A_{s2}, and the depth of each level below the top surface of the section is d_{s1} and d_{s2}, respectively.

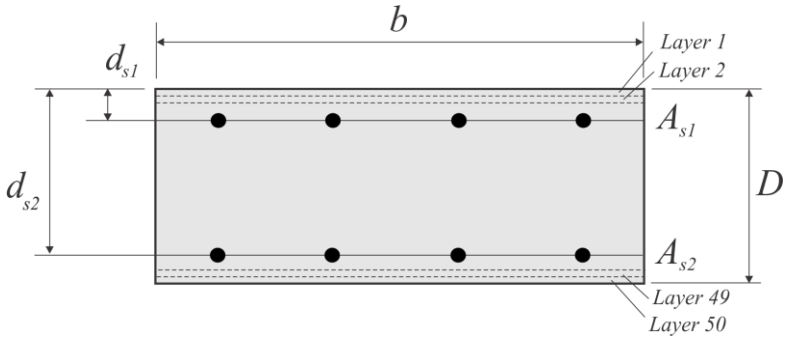

Fig. 4 Typical layered cross-section containing two levels of reinforcement.

4.3 Instantaneous cracked section analysis at first loading (τ_0):

The internal actions on the layered cross-section at time τ_0, i.e. axial force $N_{i,0}$ and moment $M_{i,0}$, are calculated by summing the contributions of each of the concrete layers and each of the steel areas. With the cross-section subdivided into 50 concrete layers, and initially assuming that all concrete layers are uncracked, the contribution of the concrete to the internal axial force ($N_{c,0}$) is:

$$N_{\mathrm{c},0} = \sum_{i=1}^{50} A_{\mathrm{c}(i)}\sigma_{\mathrm{c}(i),0} = \sum_{i=1}^{50} A_{\mathrm{c}(i)}E_{\mathrm{cc}}(\varepsilon_{\mathrm{r},0} - y_{(i)}\kappa_0) = \sum_{i=1}^{50}\left(A_{\mathrm{c}(i)}E_{\mathrm{cc}}\right)\varepsilon_{\mathrm{r},0} - \sum_{i=1}^{50}\left(B_{\mathrm{c}(i)}E_{\mathrm{cc}}\right)\kappa_0 \tag{6}$$

where $A_{c(i)}$ and $B_{c(i)}$ are the area and the first moment of area of the i-th concrete layer about the x-axis; and $y_{(i)}$ is the distance between the centroid of the i-th concrete layer and the reference axis. It is assumed that the stress in each concrete layer is uniform and corresponds to the strain at its centroid. The contribution of the concrete to the internal moment ($M_{c,0}$) is given by

$$M_{\mathrm{c},0} = \sum_{i=1}^{50} -y_{(i)}A_{\mathrm{c}(i)}\sigma_{\mathrm{c}(i),0} = \sum_{i=1}^{50} A_{\mathrm{c}(i)}E_{\mathrm{cc}}(-y_{(i)}\varepsilon_{\mathrm{r},0} + y_{(i)}^2\kappa_0) = -\sum_{i=1}^{50}\left(B_{\mathrm{c}(i)}E_{\mathrm{cc}}\right)\varepsilon_{\mathrm{r},0} + \sum_{i=1}^{50}\left(I_{\mathrm{c}(i)}E_{\mathrm{cc}}\right)\kappa_0 \tag{7}$$

where $I_{c(i)}$ is the second moment of area of the i-th concrete layer about the z-axis. The concrete rigidities for the cross-section are:

$$R_{\mathrm{A,c}} = \sum_{i=1}^{50}\left(A_{\mathrm{c}(i)}E_{\mathrm{cc}}\right);\quad R_{\mathrm{B,c}} = \sum_{i=1}^{50}\left(y_{\mathrm{c}(i)}A_{\mathrm{c}(i)}E_{\mathrm{cc}}\right);\quad R_{\mathrm{I,c}} = \sum_{i=1}^{50}\left(y_{\mathrm{c}(i)}^2A_{\mathrm{c}(i)}E_{\mathrm{cc}}\right) \qquad (8a, b, c)$$

and Eqs. 6 and 7 can be re-written as:

$$N_{\mathrm{c},0} = R_{\mathrm{A.c}}\varepsilon_{\mathrm{r},0} - R_{\mathrm{B.c}}\kappa_0 \qquad \text{and} \qquad M_{\mathrm{c},0} = -R_{\mathrm{B.c}}\varepsilon_{\mathrm{r},0} + R_{\mathrm{I.c}}\kappa_0 \qquad (9a,b)$$

Similarly, the contributions of the steel reinforcement to the internal axial force ($N_{\mathrm{s},0}$) and to the internal moment ($M_{\mathrm{s},0}$) are:

$$N_{\mathrm{s},0} = \sum_{i=1}^{2}A_{\mathrm{s}(i)}\sigma_{\mathrm{s}(i),0} = \sum_{i=1}^{2}A_{\mathrm{s}(i)}E_{\mathrm{s}}(\varepsilon_{\mathrm{r},0} - y_{\mathrm{s}(i)}\kappa_0) = \sum_{i=1}^{2}\left(A_{\mathrm{s}(i)}E_{\mathrm{s}}\right)\varepsilon_{\mathrm{r},0} - \sum_{i=1}^{2}\left(B_{\mathrm{s}(i)}E_{\mathrm{s}}\right)\kappa_0 \qquad (10)$$

$$M_{\mathrm{s},0} = \sum_{i=1}^{2} - y_{\mathrm{s}(i)}A_{\mathrm{s}(i)}\sigma_{\mathrm{s}(i),0} = \sum_{i=1}^{2}A_{\mathrm{s}(i)}E_{\mathrm{s}}(-y_{\mathrm{s}(i)}\varepsilon_{\mathrm{r},0} + y_{\mathrm{s}(i)}^2\kappa_0) = -\sum_{i=1}^{2}\left(B_{\mathrm{s}(i)}E_{\mathrm{s}}\right)\varepsilon_{\mathrm{r},0} + \sum_{i=1}^{2}\left(I_{\mathrm{s}(i)}E_{\mathrm{s}}\right)\kappa_0 \qquad (11)$$

where $A_{\mathrm{s}(i)}$, $B_{\mathrm{s}(i)}$ and $I_{\mathrm{s}(i)}$ are the area, the first moment of area and the second moment of area, respectively, of the i-th steel area about the z-axis; and $y_{\mathrm{s}(i)}$ is the y-coordinate of its centroid. Provided the steel has not yielded, the steel rigidities for the cross-section are:

$$R_{A,s} = \sum_{i=1}^{2}\left(A_{\mathrm{s}(i)}E_{s}\right);\quad R_{B,s} = \sum_{i=1}^{2}\left(y_{s(i)}A_{\mathrm{s}(i)}E_{s}\right);\quad R_{I,s} = \sum_{i=1}^{2}\left(y_{s(i)}^2A_{\mathrm{s}(i)}E_{s}\right) \qquad (12a, b, c)$$

Eqs. 10 and 11are re-written as:

$$N_{\mathrm{s},0} = R_{\mathrm{A.s}}\varepsilon_{\mathrm{r},0} - R_{\mathrm{B.s}}\kappa_0 \qquad \text{and} \qquad M_{\mathrm{s},0} = -R_{\mathrm{B.s}}\varepsilon_{r,0} + R_{\mathrm{I.s}}\kappa_0 \qquad (13a, b)$$

If the steel reinforcement has yielded, E_{s} is taken as zero in Eqs. 12. The governing equilibrium equations for a typical cross-section are therefore:

$$N_{\mathrm{i},0} = (R_{\mathrm{A,c}} + R_{\mathrm{A,s}})\varepsilon_{\mathrm{r},0} - (R_{\mathrm{B,c}} + R_{\mathrm{B,s}})\kappa_0 = N_{\mathrm{e},0} \qquad (14a)$$

$$M_{\mathrm{i},0} = -(R_{\mathrm{B,c}} + R_{\mathrm{B,s}})\varepsilon_{\mathrm{r},0} + (R_{\mathrm{I,c}} + R_{\mathrm{I,s}})\kappa_0 = M_{\mathrm{e},0} \qquad (14b)$$

where $N_{\mathrm{e},0}$ and $M_{\mathrm{e},0}$ are the external axial force and bending moment, respectively. This system of two equations can be solved to obtain the two unknowns $\varepsilon_{\mathrm{r},0}$ and κ_0. With the strain diagram thus fixed, the model then determines the stress in each concrete layer $\sigma_{\mathrm{c}(i),0}$ and the stress in each area of steel reinforcement $\sigma_{\mathrm{s}(i),0}$. If the strain at the centroid of a concrete layer is less than or equal to the cracking strain $\varepsilon_{\mathrm{t.1}}$ (see Fig. 2), the layer is uncracked and the concrete stress is $\sigma_{\mathrm{c}(i),0} = E_{\mathrm{cc}}\varepsilon_{\mathrm{c}(i),0}$. If the strain at the centroid of a concrete layer is greater than the cracking strain ($\varepsilon_{\mathrm{t.1}}$), the layer is assumed to have cracked and the concrete stress is obtained from the idealised stress-instantaneous strain curve in Fig. 2. The force in each concrete layer is $A_{\mathrm{c}(i)}\,\sigma_{\mathrm{c}(i),0}$ and the force in each steel area is $A_{\mathrm{s}(i)}\,\sigma_{\mathrm{s}(i)}$. The depth to the neutral axis is then adjusted until the sum of all the internal forces equals the external axial load, i.e. until:

$$N_{\mathrm{i},0} = \sum_{i=1}^{50}A_{\mathrm{c}(i)}\sigma_{\mathrm{c}(i),0} + \sum_{i=1}^{2}A_{\mathrm{s}(i)}\sigma_{\mathrm{s}(i)} = N_{\mathrm{e},0} \qquad (15)$$

The moment about the centroidal axis of the uncracked section caused by these internal forces ($M_{\mathrm{i},0}$) is now calculated. If $M_{\mathrm{i},0} = M_{\mathrm{e},0}$, the correct strain distribution has been determined. If $M_{\mathrm{i},0} > M_{\mathrm{e},0}$, the top fibre strain is adjusted downward and the correct neutral axis depth is again found by iteration. If $M_{\mathrm{i},0} < M_{\mathrm{e},0}$, the top fibre strain is adjusted upwards and the correct neutral axis depth is again found by iteration. The process continues until both equilibrium equations are satisfied to the desired accuracy.

4.4 Time analysis during each time interval (τ_{k-1} to τ_k):

At any time after initial loading, the elastic strain distribution (i.e. $\varepsilon_{r,k}$ and κ_k) caused by an applied axial load N and a moment M is obtained by solving the two equilibrium equations expressed as

$$\begin{bmatrix} \varepsilon_{r,k} \\ \kappa_k \end{bmatrix} = \frac{1}{R_A R_I - R_B^2} \begin{bmatrix} R_I & -R_B \\ -R_B & R_A \end{bmatrix} \begin{bmatrix} N \\ M \end{bmatrix} \tag{16}$$

That is

$$\varepsilon_{r.k} = \frac{R_I}{R_A R_I - R_B^2} N + \frac{-R_B}{R_A R_I - R_B^2} M \quad \textit{and} \quad \kappa_k = \frac{-R_B}{R_A R_I - R_B^2} N + \frac{R_A}{R_A R_I - R_B^2} M \tag{17a,b}$$

During each time interval, a *relaxation procedure* is adopted to determine the change of strains and stresses caused by creep and shrinkage. The strain state is initially *frozen*, i.e. the strain distribution existing at the start of the time interval is initially assumed to remain unchanged. If the total strain in a concrete layer is held constant and the creep and shrinkage components are allowed to develop freely, then the instantaneous component of strain must also change by an equal and opposite amount. The unrestrained creep strain that occurs in a particular layer during the time interval τ_{k-1} to τ_k is the creep strain that develops due to the initial stress τ_0 in the layer at time τ_0 and the creep caused by the stress increments that have developed in each previous time interval. This unrestrained creep strain in each layer is added to the free shrinkage that develops in the time interval and the sum is equal and opposite to the change in elastic strain.

As the instantaneous strain changes, so too does the concrete stress. As a result, the force in the concrete in each layer changes and equilibrium is not maintained. In the i-th concrete layer, with centroid d_i below the top of the cross-section, the force changes by ΔN_i and this change of force causes a bending moment about the centroidal axis of $\Delta M_i = \Delta N_i(d_i - d_{centroid})$. To restore equilibrium of the cross-section, an axial force of magnitude ΣN and a bending moment of magnitude ΣM must be applied to the cross-section, where

$$\Sigma N = \sum_{i=1}^{50} \Delta N_i \quad \text{and} \quad \Sigma M = \sum_{i=1}^{50} \Delta M_i \tag{18a, b}$$

The change of strain due to creep and shrinkage in each layer is considered to be artificially prevented by restraining actions $-\Sigma N$ and $-\Sigma M$. When ΣN and ΣM are applied to the section, the restraining actions are removed and equilibrium is restored. The strains resulting from ΣN and ΣM are calculated using Eq. 17a and 17b.The change in stress during the time interval in each concrete layer is the loss of stress that occurs while the strain state is frozen plus the stress that is induced by ΣN and ΣM. The change in stress during the time interval in each steel bar is induced by ΣN and ΣM.

In the layered model presented here, an increment of stress is applied to each concrete layer at each time instant due to the internal restraint provided by the bonded reinforcement and adjacent concrete layers. In any layer, each stress increment is associated with a different creep coefficient depending on the time at which the increment is applied. In the current analysis, the final creep coefficients $\varphi^*_{cc}(\tau_k)$ and $\varphi^*_{cf.av}(\tau_k)$ associated with stress increments applied at τ_0 to τ_9 for both the uncracked and cracked layers are required as input data. The changes in each creep coefficient during each successive time interval are assumed to be equal. The shrinkage strain that develops in the concrete during each time interval is also required as input.

The unrestrained creep and shrinkage strains that develop in the i-th uncracked layer in the first time step (τ_0 to τ_1) are $\Delta\varepsilon_{cc(i).1} = \varepsilon_{cc(i).2}\,\varphi_{cc}(\tau_1, \tau_0)/E_{cc}$ and $\varepsilon_{cs.1} = \varepsilon_{cs}(\tau_1)$ where $\varphi_{cc}(\tau_1, \tau_0)$ is the creep coefficient of the uncracked concrete at τ_1 due to a stress applied at τ_0. In the 2nd time step (τ_1 to τ_2),

$\Delta\varepsilon_{cc(i).2} = \sigma_{c(i),0}[\varphi_{cc}(\tau_2,\tau_0)-\varphi_{cc}(\tau_1,\tau_0)]/E_{cc} + (\sigma_{c(i),1}-\sigma_{c(i),0})\varphi_{cc}(\tau_2,\tau_1)/E_{cc}$ and $\varepsilon_{cs.2} = \varepsilon_{cs}(\tau_2) - \varepsilon_{cs}(\tau_1)$. In the tenth and final time step (τ_9 to τ_{10}):

$$\begin{aligned}\Delta\varepsilon_{cc(i).10} = {} & \sigma_{c(i),0}[\varphi_{cc}(\tau_{10},\tau_0) - \varphi_{cc}(\tau_9,\tau_0)]/E_{cc} + (\sigma_{c(i),1} - \sigma_{c(i),0})[\varphi_{cc}(\tau_{10},\tau_1)-\varphi_{cc}(\tau_9,\tau_1)]/E_{cc} + \\ & (\sigma_{c(i),2}-\sigma_{c(i),1})[\varphi_{cc}(\tau_{10},\tau_2)-\varphi_{cc}(\tau_9,\tau_2)]/E_{cc} + (\sigma_{c(i),3}-\sigma_{c(i),2})[\varphi_{cc}(\tau_{10},\tau_3)-\varphi_{cc}(\tau_9,\tau_3)]/E_{cc} + \\ & (\sigma_{c(i),4}-\sigma_{c(i),3})[\varphi_{cc}(\tau_{10},\tau_4)-\varphi_{cc}(\tau_9,\tau_4)]/E_{cc} + (\sigma_{c(i),5}-\sigma_{c(i),4})[\varphi_{cc}(\tau_{10},\tau_5)-\varphi_{cc}(\tau_9,\tau_5)]/E_{cc} + \\ & (\sigma_{c(i),6}-\sigma_{c(i),5})[\varphi_{cc}(\tau_{10},\tau_6)-\varphi_{cc}(\tau_9,\tau_6)]/E_{cc} + (\sigma_{c(i),7}-\sigma_{c(i),6})[\varphi_{cc}(\tau_{10},\tau_7)-\varphi_{cc}(\tau_9,\tau_7)]/E_{cc} + \\ & (\sigma_{c(i),8}-\sigma_{c(i),7})[\varphi_{cc}(\tau_{10},\tau_8)-\varphi_{cc}(\tau_9,\tau_8)]/E_{cc} + (\sigma_{c(i),9}-\sigma_{c(i),8})\varphi_{cc}(\tau_{10},\tau_9)/E_{cc}\end{aligned}$$

For the cracked layers, simply replace $\varphi_{cf.av}(\tau_j,\tau_k)$ for $\varphi_{cc}(\tau_j,\tau_k)$ and the appropriate value of E_{ft} for E_{cc} in the above equations.

The sum of the free creep plus shrinkage strains that have developed in each layer during a typical time interval is equal and opposite to the change in elastic strain that occurs in that layer while the strain is initially held constant. The change in elastic strain in each layer is associated with a change in stress. When the sum of axial forces ΣN and sum of moments about the z-axis ΣM that have occurred are applied to the cross-section to re-establish equilibrium, the increments of strain at the reference axis and curvature that occur during the time interval are determined using Eqs. 17a and 17b. The concrete stress at the end of the time step (at τ_k) is the sum of the stress at τ_{k-1}, the change in stress due to the restraining force in the layer $-\Sigma$N and the stress in the layer caused by ΣN and ΣM. The stress in the reinforcement at the end of the time step (at τ_k) is the sum of the stress at τ_{k-1} and the stress in the steel caused by ΣN and ΣM.

At each time instant, τ_0 to τ_{10}, the strains and stresses at the centroid of each concrete layer and in each reinforcement bar are determined, as well as the top and bottom fibre stresses in the uncracked and cracked parts of the concrete cross-section.

5. Estimation of Crack Width

The maximum crack width w_{max} at the tensile face of a fibre-reinforced concrete member any time t is approximately equal to the mean strain at the tensile face ε_t times the maximum crack spacing s_r [4, 7], i.e. $w_{max} = s_r \varepsilon_t$. The maximum crack spacing s_r is also related to the macro synthetic fibre content ρ_f. For various quantities of Barchip macro-synthetic fibres, the maximum crack spacing s_r has been observed experimentally [11] to be approximated by the expression:

$$s_r = (1- 0.05\rho_f)\, s_{r.max} \approx 0.8\,(1- 0.05\rho_f) D \geq 0.4\, D \qquad (19)$$

where ρ_f is in kg/m^3, $s_{r.max}$ is the maximum crack spacing determined for a conventionally reinforced cross-section by Eurocode 2 [7], and D is the overall depth of the cross-section.

6. Results of Some Example Analyses

6.1 Cross-section

In this section, the results of a number of cross-sectional analyses are presented. Referring to the cross-section of Fig. 4, D = 300 mm, b = 1000 mm, d_{s1} = 50 mm and d_{s2} = 250 mm. The cross-section is subjected to various combinations of axial force and moment applied at τ_0. The variables considered, in addition to the applied actions, are the fibre content ρ_f , residual tension after cracking ($f'_{t,r}$), the area of compressive and tensile steel A_{s1} and A_{s2} and the creep coefficient for the cracked fibres, $\varphi_{cf.av}$.

6.2 Material Properties

According to AS3600-2009 [5], for 50 MPa concrete, the final creep coefficient (at age 1000 days) for a 300 mm thick uncracked slab or wall section may be taken as $\varphi_{cc}^*(\tau) = 3.93/(1+ \log\tau)$ and

the final shrinkage strain is $\varepsilon^*_{cs} = -0.0005$. Unless stated otherwise, the material properties assumed in the analyses are as follows:

f'_c = 50 MPa; $f'_t = 0.6\sqrt{f'_c}$ = 4.243 MPa; $E_{cc} = E_{ct}$ = 34800 MPa; ρ_f = 3 kg/m^3 ($f'_{t.r} = 0.2 f'_t$); E_s = 200000 MPa, f_{sy} = 500 MPa; $\varepsilon_{t.1} = f'_t / E_{ct}$ = 0.0001219; $\varepsilon^*_{cs} = -0.0005$. The creep coefficients $\varphi_{cc}^*(\tau_k)$ for the concrete are as listed in Table 1 with $\varphi_{cf.av}^*(\tau_k)$ assumed to be $5\varphi_{cc}^*(\tau_k)$.

Table 1. Creep coefficients for concrete out to 1000 days.

τ (days)	τ_0 = 7	τ_1 =13	τ_2 =23	τ_3 = 37	τ_4 =58	τ_5 = 86	τ_6 =129	τ_7 =194	τ_8 =302	τ_9 =508	τ_{10} =1000
$\varphi_{cc}^*(\tau_k)$	2.13	1.86	1.66	1.53	1.41	1.33	1.24	1.16	1.08	0.95	0

6.3 Short-term moment versus average curvature relationships

6.3.1 Cross-section containing equal top and bottom reinforcement

The effect of varying the fibre content (ρ_f) on the instantaneous moment versus average curvature relationship of a cross-section containing $A_{s1} = A_{s2}$ = 1000 mm^2 is shown in Fig. 5 (for N_e = -300 kN). The cross-section is subjected to monotonically increasing bending deformation with constant axial force. Three different values of fibre content are considered: (i) ρ_f = 0 ($f'_{t.r}$ = 0); (ii) ρ_f = 3 kg/m^3 ($f'_{t.r} = 0.2 f'_t$); and (iii) ρ_f = 6 kg/m^3 ($f'_{t.r} = 0.4 f'_t$). For each combination of variables, the short-term cracked section analysis has been performed for the full range of moments. Cracking first occurred at points *A*. Yielding of the bottom reinforcing steel in tension occurred at point *B* on each curve. Note that the fibres increase the post-cracking stiffness significantly and also increase the peak moment that the section can carry. In practice, for a particular fibre type and quantity, testing is required to determine the correct value of $f'_{t.r}$.

6.3.2 Effect of varying the quantity of reinforcement:

The effect of including various quantities of reinforcement on the short-term moment vs average curvature relationship of a doubly reinforced cross-section is shown in Fig. 6. The cross-section contains equal quantities of tensile and compressive steel ($A_{s1} = A_{s2}$) and the steel areas are as follows: $A_{s1} = A_{s2}$ = 0, 500, 1000 and 1500 mm^2. In all cases, the cross-section is subjected to increasing bending deformation with a constant axial force of N_e = -300 kN. The fibre content ρ_f = 3 kg/m^3 ($f'_{t.r} = 0.2 f'_t$). In addition to increasing the ultimate strength of the cross-section, the inclusion of additional tensile reinforcement increases the post-cracking stiffness of the cross-section (as expected).

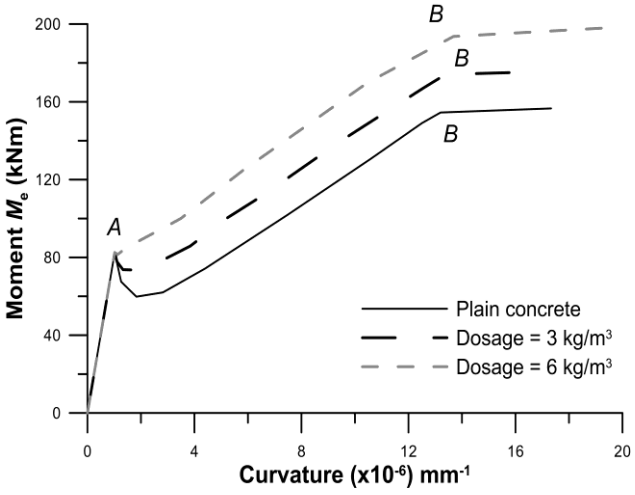

Fig. 5 Effect of residual tension in fibres after cracking on the short-term moment vs curvature relationships for a section with $A_{s1} = A_{s2}$ = 1000 mm^2 and N_e = -300 kN.

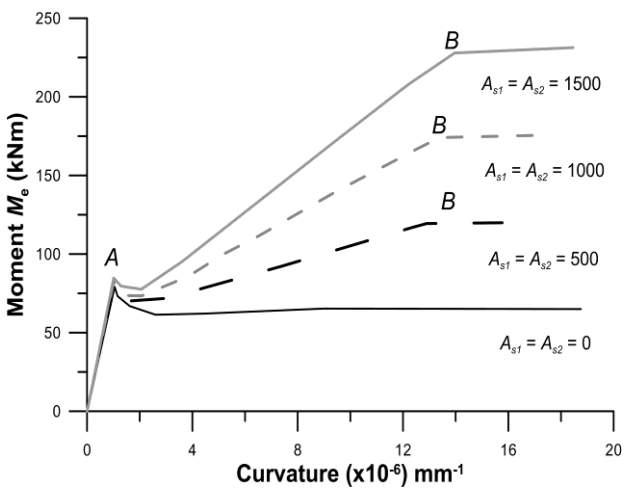

Fig. 6 Effect of increasing the quantity of tensile reinforcement on the short-term moment vs curvature relationship ($A_{s1} = A_{s2}$, N_e = -300 kN, ρ_f = 3 kg/m^3)

6.3.3 Unreinforced Cross-section

The effect of varying the fibre quantity on the post-cracking moment-curvature relationship of an unreinforced concrete cross-section (i.e. A_{s1} = A_{s2} = 0) is shown in Fig. 7 for two different levels of axial compression (N_e = -100 or -300 kN). Two different fibre quantities are considered, namely ρ_f = 3 kg/m^3 ($f'_{t.r} = 0.2 f'_t$) represented by solid lines, and ρ_f = 6 kg/m^3 ($f'_{t.r} = 0.4 f'_t$) represented by the dashed lines.

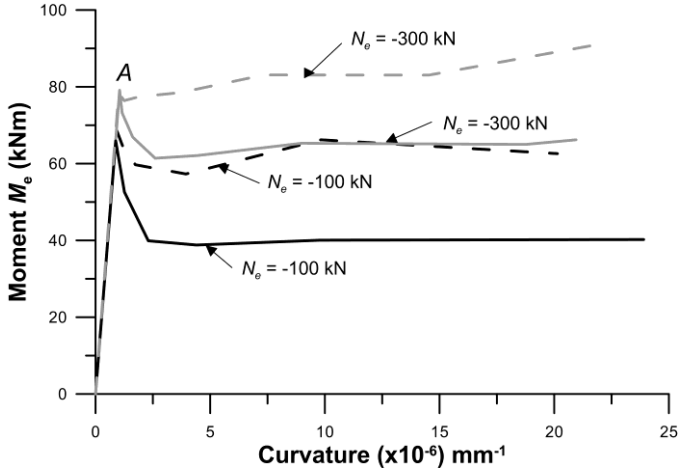

Fig. 7 Effect of residual tension (fibre content) after cracking on the short-term moment vs curvature relationships for an unreinforced section (A_{s1}= A_{s2}= 0).

6.4 Stress in tensile reinforcement and maximum crack width at first loading

The effect of varying the fibre content on the stress in the tensile reinforcement in a cross-section containing A_{s1} = A_{s2} = 1000 mm^2 is shown in Fig. 8 (where the axial force N_e = -300 kN). Fibre content has a marked effect on the instantaneous stress in the tensile steel after cracking and on the maximum instantaneous crack width. For example, at a moment level of M_e = 100 kNm, when the fibre content is zero, the tensile steel stress is 266 MPa and the maximum crack width is 0.407 mm. When the fibre content is ρ_f = 3 kg/m^3 ($f'_{t.r} = 0.2 f'_t$), the tensile steel stress and the maximum crack width reduce to 173.7 MPa and 0.23 mm, respectively. When the fibre content is ρ_f = 6 kg/m^3 ($f'_{t.r} = 0.4 f'_t$), the tensile steel stress and maximum crack width reduce further to 103.0 MPa and 0.12 mm, respectively. For a given concrete cover to the tensile reinforcement, the maximum flexural crack width is taken to be proportional to the product of crack spacing and the average tensile strain at the tensile face of the cross-section. The fibres not only reduce the tensile strain, but also the crack spacing [11]. In the analyses presented in Fig. 7, at an applied moment of 100 kNm, the addition of 3 kg/m^3 and 6 kg/m^3 of fibres causes the maximum crack width to reduce to 56.5% and 29.5%, respectively, of the width of cracks in a similar beam-column without fibres.

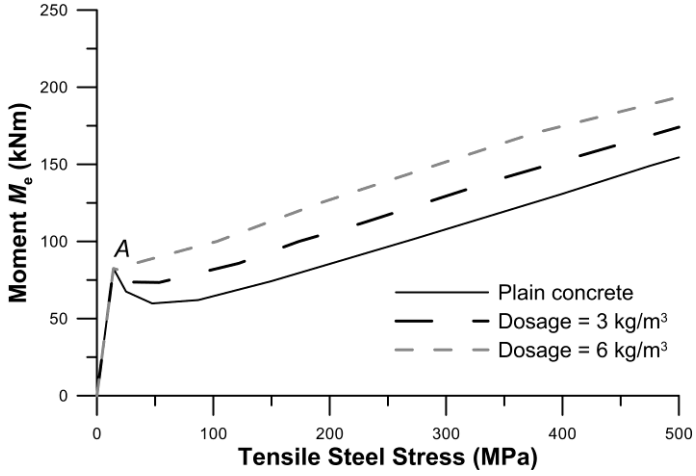

Fig. 8 Effect of fibre content on the stress in the bottom tensile reinforcement for a section with A_{s1} = A_{s2} = 1000 mm^2 and N_e = -300 kN.

6.5 Effect of Reinforcement Quantities on Curvature and Crack Width Versus Time

6.5.1 Reinforcement

Fig. 9 shows curvature versus time curves for cross-sections with A_{s1} = A_{s2} = 500, 1000 and 1500mm^2. The applied moment and axial force are M_e = 100 kNm and N_e = -300 kN. The fibre content is ρ_f = 3 kg/m^3 ($f'_{t.r} = 0.2 f'_t$). Fig. 10 shows the corresponding development of maximum crack width with time. The inclusion of additional bar reinforcement significantly reduces both the instantaneous and time-dependent curvature. It also significantly reduces the maximum crack width.

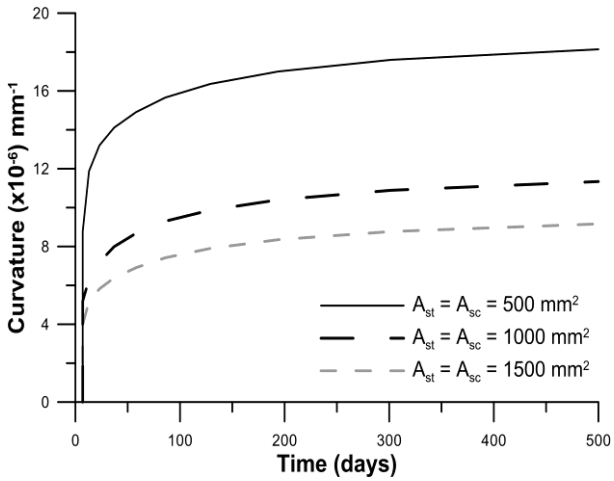

Fig. 9 Effect of bar reinforcement quantity on the time-varying curvature (M_e = 100 kNm, N_e = -300 kN, ρ_f = 3 kg/m^3, creep ratio = 5).

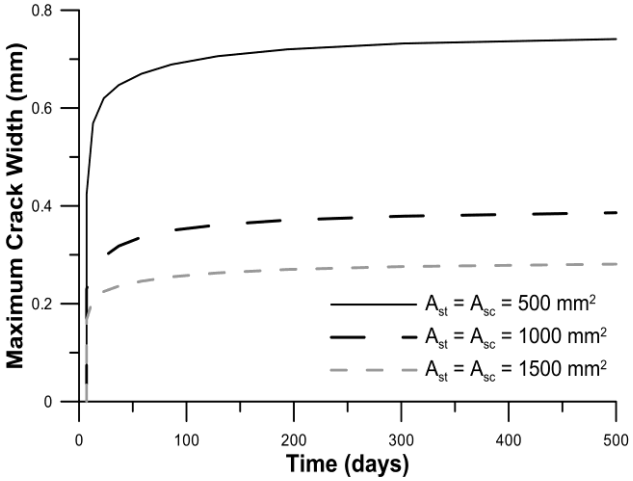

Fig. 10 Effect of bar reinforcement quantity on the time-varying crack width (M_e = 100 kNm, N_e = -300 kN, ρ_f = 3 kg/m^3, creep ratio = 5).

6.5.2 Fibre Content

Fig. 11 shows the average curvature versus time curves for cross-sections with fibre content of ρ_f = 0, ρ_f = 3 kg/m^3 and ρ_f = 6 kg/m^3. The cross-section contains A_{s1} = A_{s2} = 1000 mm^2 and was subjected to an axial load N_e = -300 kN and a bending moment of M_e = 100 kNm. For each analysis the average creep in the cracked fibre reinforced concrete in tension was taken to be five the magnitude of the creep of concrete in compression. Fig. 12 shows the corresponding change in maximum crack width with time. The inclusion of fibres reduces the curvature at any time after loading and has a marked effect on the maximum crack width. The inclusion of 6 kg/m^{3}of fibres reduces the final crack width by a factor of about two.

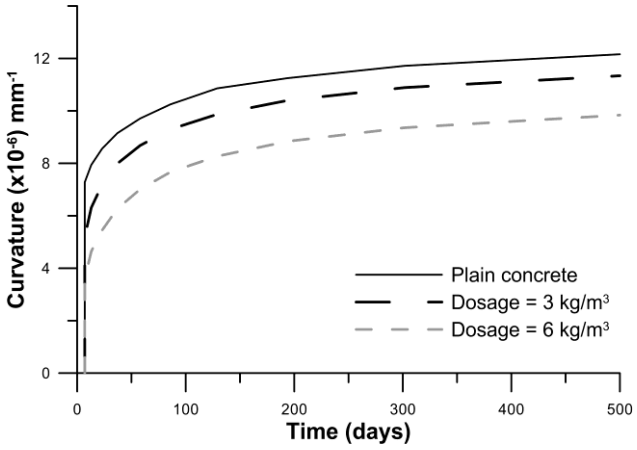

Fig. 11 Effect of fibre content on the time-varying curvature (A_{s1} = A_{s2} = 1000 mm^2 , M_e = 100 kNm, N_e = -300 kN, creep ratio = 5)

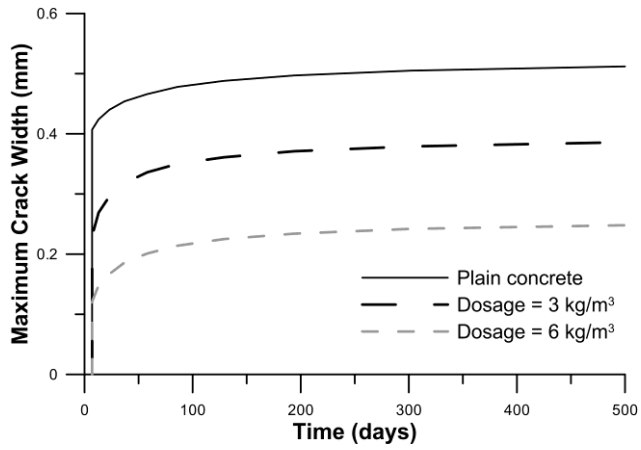

Fig. 12 Effect of fibre content on the maximum crack width (A_{s1} = A_{s2} = 1000 mm^2, M_e = 100 kNm, N_e = -300 kN, creep ratio = 5)

5.5.3 Fibre Creep Factor

The effect of varying the average creep coefficient for the cracked fibre reinforced concrete in tension is shown in Fig 13 and Fig. 14. The cross-section contains A_{s1} = A_{s2} = 1000 mm^2, has a fibre content of ρ_f = 3 kg/m^3 and is subjected to an axial load N_e = -300 kN and a bending moment of M_e = 100 kNm. The ratio of the creep coefficient of the cracked fibre reinforced concrete in tension to the creep coefficient of the uncracked concrete is taken as either 2, 5 or 10. The magnitude of the creep of the cracked fibre concrete has a relatively small effect on curvature and crack width.

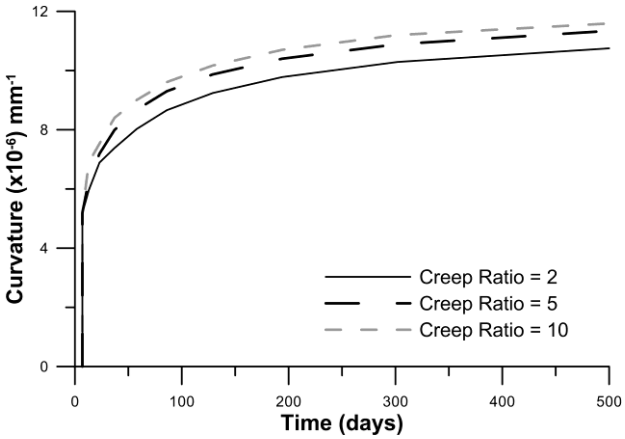

Fig. 13 Effect of fibre creep on the time-varying curvature (A_{s1} = A_{s2} = 1000 mm^2, ρ_f = 3 kg/m^3 , N_e = -300 kN and M_e = 100 kNm).

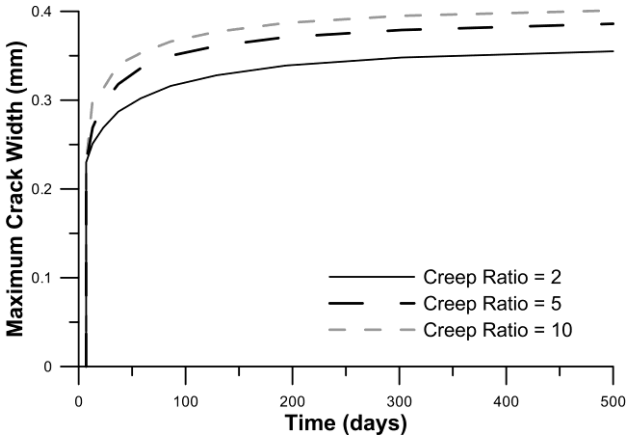

Fig. 14 Effect of fibre creep on the time-varying maximum crack width (A_{s1} = A_{s2} = 1000 mm^2, ρ_f = 3 kg/m^3, N_e = -300 kN and M_e = 100 kNm.

6.6 Typical redistribution of stress and strain with time on a cross-section

The strain and stress distribution on the cross section, with A_{s1} = 1000 mm^2 and A_{s2} = 1000 mm^2, when subjected to an applied moment M_e = 100 kNm and an applied axial force N_e = -300 kN, are shown for different fibre contents in Fig. 15. The fibre content is ρ_f = 0 in Fig. 15a, ρ_f = 3 kg/m^3 ($f'_{t.r} = 0.2 f'_t$) in Fig. 15b and ρ_f = 6 kg/m^3 ($f'_{t.r} = 0.4 f'_t$) in Fig. 15c. In each case, the creep coefficient of the cracked fibre reinforced concrete in tension is five times the creep coefficient of the uncracked concrete, i.e. $\varphi_{cf.av}/\varphi_{cc}$= 5.

In Fig. 15b, for example, with ρ_f = 3 kg/m^3, the depth to the neutral axis at first loading is 82.7 mm and the depth of the uncracked part of the concrete is 107.7 mm, as shown. From τ_0 to τ_{10}, the curvature increases from 5.19 x 10^{-6} mm^{-1} to 11.74 x 10^{-6} mm^{-1}; the top fibre compressive stress reduces from -14.94 MPa to -9.81 MPa; the stress in the tensile steel increases from 173.6 MPa to 265.9 MPa. The residual tension at the bottom of the cross-section in the cracked fibre reinforced tensile concrete reduces with time from +0.79 MPa to +0.28 MPa. The addition of fibres reduces the curvature and reduces the average bottom fibre strain and tensile steel stress, thereby significantly reducing flexural crack widths.

6.7 Effect of axial force on the redistribution of stress and strain with time:

The effect of axial load on the instantaneous and long-term stress and strain distributions on a cross-section containing A_{sc} = A_{st} = 1000 mm^2 and subjected to M_e = 100 kNm is examined here. The fibre content is ρ_f = 6 kg/m^3 and the creep ratio $\varphi_{cf.av}/\varphi_{cc}$= 5. Fig. 16 shows the strain distributions for three different axial load levels, N_e = 0 kN , N_e = -300 kN, and N_e = -600 kN at both τ_0 and τ_{10} together with the corresponding stress distributions (solid lines represent τ_0 and dashed lines represent τ_{10}). Crack widths for these cases were 0.314 mm, 0.116 mm and 0.029 mm in the short term and 0.450 mm, 0.243 mm and 0.0 mm in the long term for the three cases N_e = 0 kN , N_e = -300 kN, and N_e = -600 kN, respectively. In the last case, the stress in the concrete at the base of the section remains in tension while the steel is in compression primarily because long-term shrinkage induces tension in the concrete in addition to the strains induced by the axial load and moment.

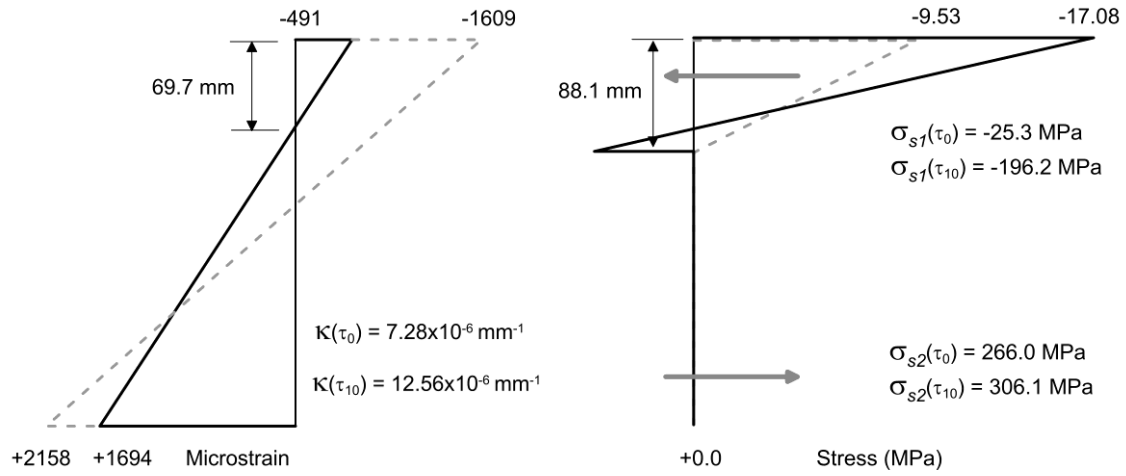

a) Fibre dosage 0 kg/m^3

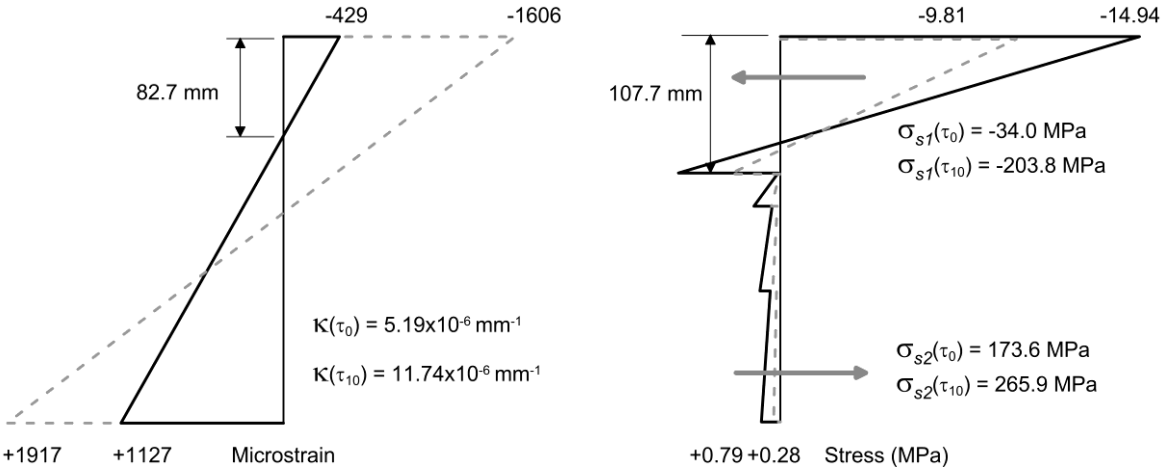

b) Fibre dosage 3 kg/m^3, $f'_{t.r} = 0.2\,f'_t$

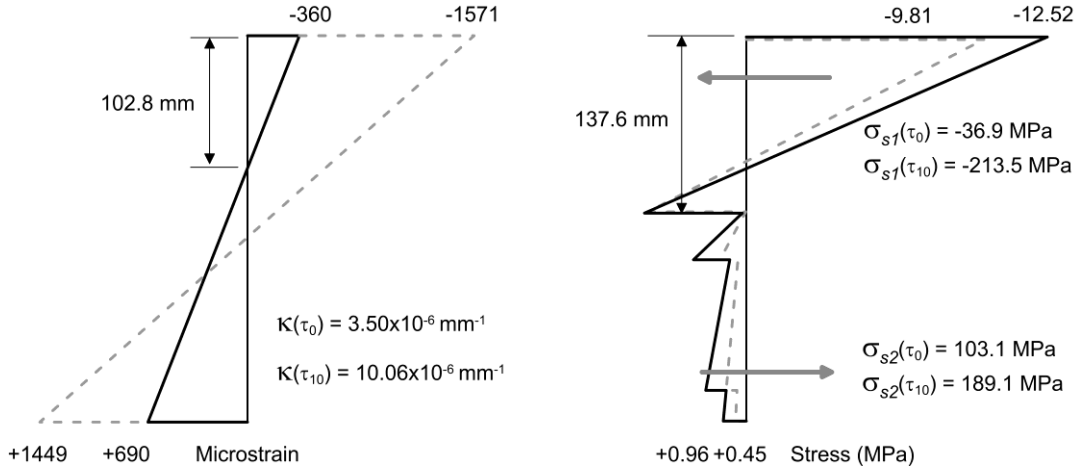

c) Fibre dosage 6 kg/m^3, $f'_{t.r} = 0.4\,f'_t$

Fig. 15 Strain and stress distributions on a cracked cross-section at times τ_0 and τ_{10} (with A_{s1} = A_{s2} = 1000 mm^2; M_e = 100 kNm; N_e = -300 kN). Solid lines represent τ_0 and dashed lines represent τ_{10}.

In reality, most axial loads on tunnel segments are larger than assumed here, so no cracks will occur in service and the creep properties of the fibres in tension are irrelevant.

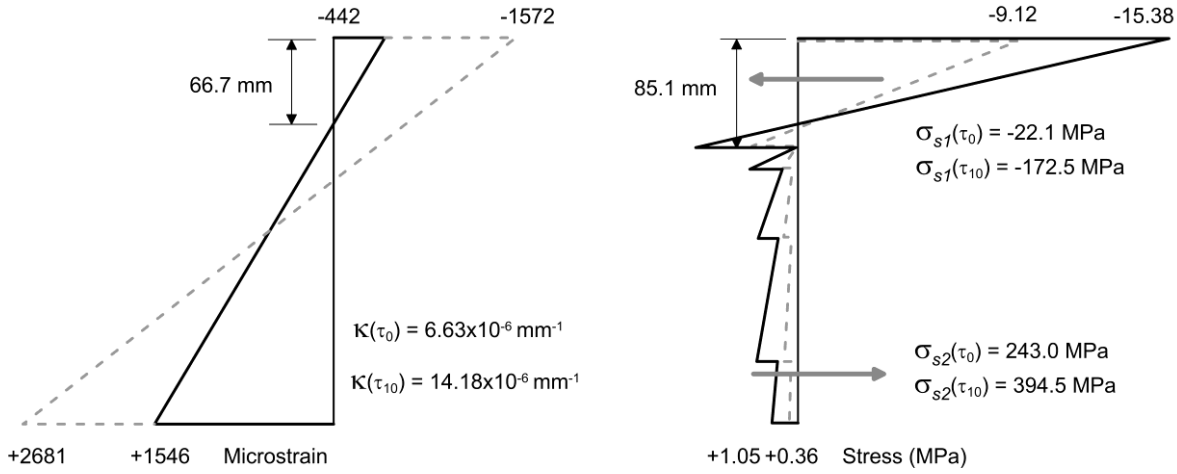

a) Strain and stress distributions for N_e = 0 kN.

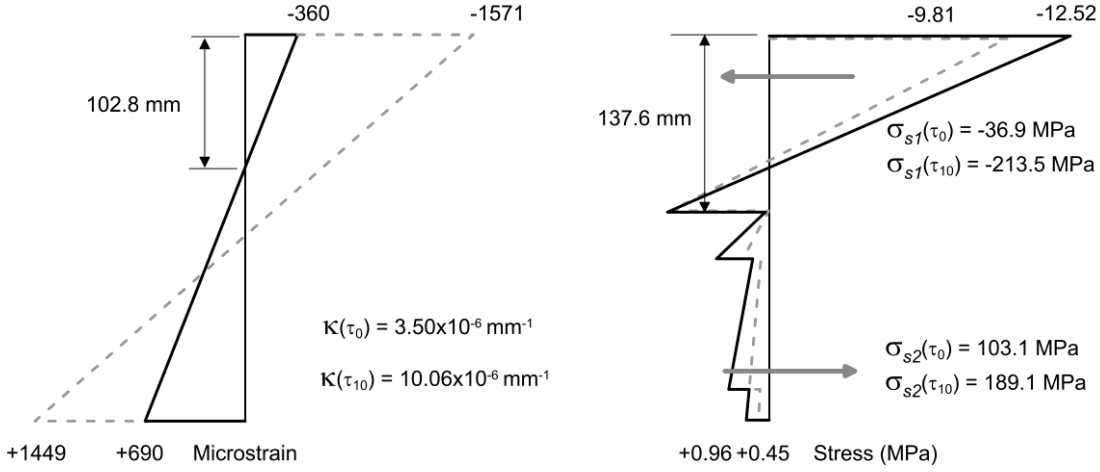

b) Strain and stress distributions for N_e = -300 kN.

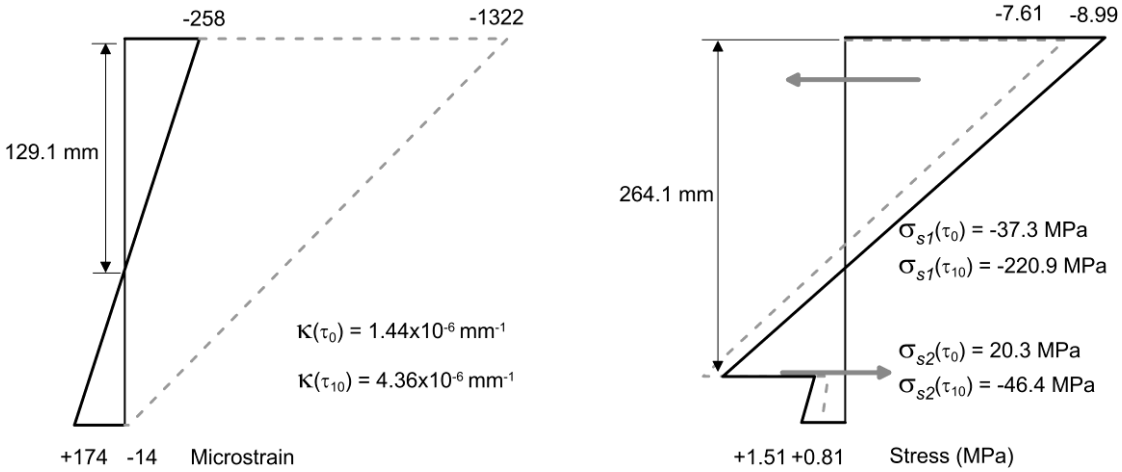

c) Strain and stress distributions for N_e = -600 kN.

Fig. 16 Effect of axial load on the strain and stress distributions at times τ_0 and τ_{10} (with A_{s1} = A_{s2} = 1000 mm^2; M_e = 100 kNm; ρ_f = 6 kg/m^3)

7. Concluding Remarks

A method to determine the effects of creep and shrinkage on the time-dependent behaviour of cracked, macro-synthetic fibre reinforced concrete cross-sections containing conventional bar reinforcement subjected to a sustained bending moment and axial force is presented. The method can be applied to any combination of fibres, concrete, and conventional steel reinforcement in a

tunnel lining, be it composed of shotcrete, cast-in-place concrete, or pre-cast segments. The analysis procedure is outlined and involves geometric and temporal discretisation. The procedure has been implemented in a spreadsheet and is illustrated by several examples. The inclusion of macro-synthetic fibres in the concrete has only a minor effect on the flexural strength of the cross-section, but the fibres reduce time-dependent in-service deformations and significantly reduce maximum crack widths when used in combination with conventional reinforcing bars. These outcomes indicate that macro-synthetic fibres are a useful means of improving the performance of conventionally reinforced tunnel linings if cracks are likely in service. They can also be used on their own as reinforcement when moderate bending moments occur in combination with high sustained axial loading.

References

[1] CNR DT 204 (2006). *Guide for the design and construction of fibre reinforced concrete structures*, Advisory Committee on Technical Recommendations for Construction, Rome.
[2] DBV Guide to Good Practice, (2001) *Steel Fibre Concrete*. Deutscher Beton- und Bautechnik-Verein, Berlin.
[3] Edition October 2012, fib *Model Code 2010*, (2012), Bulletin 65, Fèdération Internationale du Béton, Lausanne.
[4] Gilbert RI and Ranzi G (2011). *Time-dependent behaviour of concrete structures*. Spon Press. London.
[5] AS 3600 (2009). *Concrete Structures*, Standards Australia, Sydney.
[6] ACI 318M-11 (2011). *Building code requirements for reinforced concrete and Commentary*. American Concrete Institute, Farmington Hills, MI.
[7] EN 1992-1-1: (2004) Eurocode 2: *Design of concrete structures* Part 1-1: General rules and rules for buildings.
[8] Neville, A.M., Dilger, W.H. and Brooks, J.J. (1983). *Creep of Plain and Structural Concrete. Construction Press* (Longman Group Ltd), 361 pp.
[9] Bazant, Z.P., Wittmann, F.H. (eds) (1983). *Creep and Shrinkage in Concrete Structures*. John Wiley and Sons Ltd.
[10] ACI Committee 209 (2008). *Guide for modeling and calculating shrinkage and creep in hardened concrete* (ACI 209.2R-8). American Concrete Institute, Farmington Hills, Michigan, 44 pp.
[11] Bernard, E.S., (2015). "Investigation of Crack Width Control Using Barchip Fibres in Reinforced Concrete Beams", *TSE Report 248*, TSE Pty Ltd, Sydney.